Bull. Nov. Comp. Center, Math. Model. in Geoph., 17 (2014), 73–84

Properties of the inverse problem operator for reconstructing the tsunami source*

T.A. Voronina, V.V. Voronin

1. Introduction

This paper outlines some aspects of an approach to reconstructing an initial water elevation field that generates a tsunami. Recently, the devastating tsunamis have acutely put forward the problem for their timely warning and, as consequence, the importance of the accurate tsunami simulation. Mathematical modeling of tsunamis is to provide tsunami-withstanding communities with reliable information of inundation heights and arrival times for the purpose to immediate protective measures. Numerical modeling of a tsunami source is an important tool of assessment and mitigation of the negative effects of tsunamis.

Among mathematical approaches based on the inversion of near-field water-level data, most often used are the methods relying upon Green's functions technique (GFT) [1], the least square inversion combined with the GFT [3] or an optimization approach [2]. These methodologies with various modifications are widely used in practice.

This paper deals with an application of an original approach to the problem of retrieving the initial water elevation field (*tsunami source*) based on the inversion of remote measurements of water-level data (*marigrams*). This inversion method was first proposed by T.A. Voronina and V.A. Tcheverda in 1998 [4] and was already described in its fundamentals in previous papers [5, 7, 8]. Particularly, the proof of the compactness of the inverse problem operator was first presented in [5]. In this method, the data space consists of a given number of tide-gauge records, and the model parameter space is represented by the values of the initial water elevation field at a given number of points.

The direct problem of the tsunami wave propagation is considered within the scope of the linear shallow-water theory. The ill-posed inverse problem of reconstructing initial tsunami waveforms is regularized by means of the least-square inversion using the truncated SVD approach. As a result of the numerical process, an $\boldsymbol{r}$-solution is obtained [6]. In the present paper, the properties of inverting operator are studied by means of numerical modeling.

*Supported by the Russian Foundation for Basic Research under Grant 12-07-00406, by the Siberian Branch of the RAS (Project 117) and the Far-East Branch of the RAS (Project 37).

This study is aimed at investigation of the characteristics of the method avoiding the influence of such a factor as bathymetry and deals, particularly, with establishing the dependence of the goodness of the inversion on the number of receivers, their azimuthal coverage and the frequency band when the computational domain is a right-angle basin. The method presented allows one to control the instability of the numerical solution and to obtain an acceptable result in spite of the ill-posedness of the problem.

2. Models

Mathematically, the problem of reconstructing the initial tsunami waveform in the source area is formulated as determination of spatial distribution of an oscillation source using remote measurements on a finite set of points (later called *receivers*). Let us consider the coordinate system xyz and direct the axis-z downwards. The plane $\{z = 0\}$ corresponds to the undisturbed water surface. The curvature of the Earth is neglected. Consider the aquatic part Φ of a rectangular domain $\Pi = \{(x, y) : \ 0 \le x \le X, \ 0 \le y \le Y\}$ on the plane $\{z = 0\}$ with the solid boundaries Γ and the straight-line sea boundaries. The arrival of the wave on the coast is not considered in this study. One of the main advantages of this method is that it is completely independent of any particular source model. Let $\Omega = \{(x, y) : \ x_1 \le x \le x_M, \ y_1 \le y \le y_N\}$ be a tsunami source subdomain of Φ. The observational data are the water level records which are assumed to be known at a set of points in the domain Φ. Since a tsunami in the ocean is a long gravitational wave with a low amplitude, its propagation can be considered in the scope of the linear shallow water theory. Let $\eta(x, y, t)$ be a function of the water surface elevation relative to the mean sea level which is considered to be a solution of the linear shallow water equation

$$\eta_{tt} = \operatorname{div}(gh(x, y) \operatorname{grad} \eta) + f_{tt}(x, y, t) \tag{1}$$

with the initial conditions

$$\eta|_{t=0} = 0, \quad \eta_t|_{t=0} = 0 \tag{2}$$

completed on the continental coasts with the total reflecting conditions

$$\frac{\partial \eta}{\partial n}\Big|_{\Gamma} = 0, \tag{3}$$

and the boundary conditions simulated on an open boundary when the spatial boundary occurs in an ocean location. The full absorbing boundary conditions of second order of accuracy were used at the open boundary. The tsunami wave is assumed to be triggered by a sudden vertical displacement $f(x, y, t)$ of the sea floor. It is assumed that $f(x, y, t) = H(t)\varphi(x, y)$,

where $\varphi(x,y)$ is a co-seismic vertical displacement and $H(t)$ is the Heaviside step function. As a result $\varphi(x,y)$ is the initial sea surface deformation in the target domain Ω. Let us consider a special case for the approach proposed when the basin depth is the function $h(x,y)=h_0$. The acceleration of gravity is the constant g and the wave phase velocity is defined as $c(x,y)=\sqrt{gh_0}$. In addition, the function $\eta(x,y,t)$ is assumed to be known at a set of points $M_i=\{(x_i,y_i),\ i=1,\dots,P\}$. In order to obtain a system of linear algebraic equations by means of a projective method, a trigonometric basis was chosen in the model space, i.e., the unknown function $\varphi(x,y)$ was sought for as a series of spatial harmonics $\varphi_{mn}(x,y)=\sin\frac{m\pi}{l_1}(x-x_1)\cdot\sin\frac{n\pi}{l_2}(y-y_1)$, $m=1,2,\dots,M$, $n=1,2,\dots,N$, and the center of the tsunami source was believed to be at the point (x_c,y_c), being the central point of Ω. Here $l_1=(x_M-x_1)$, $l_2=(y_N-y_1)$. Thus, the unknown function of water surface elevation $\varphi(x,y)$ is approximated by the sum of spatial harmonics:

$$\varphi(x,y)=\sum_{m=1}^{M}\sum_{n=1}^{N}c_{mn}\sin\frac{m\pi}{l_1}(x-x_1)\cdot\sin\frac{n\pi}{l_2}(y-y_1) \tag{4}$$

with unknown coefficients $\{c_{mn}\}$ in the domain Ω. For sampling the initial field data, we assumed the synthetic *marigrams* to be known at the set of points $\{(x_p,y_p),\ p=1,\dots,P\}$ and for a finite number of the frequency instants K_w. Now, we assume that the dimensions of the model space and the data space are equal to

$$\dim(\text{sol})=K=MN;\quad \dim(\text{data})=L=PK_w.$$

Case study: a constant basin depth. Let us consider a special case for the approach proposed when the computational domain is the right-angle basin based on the rectangular Π (Section 2) with the height h_0, boundary condition (2) being correct for the line $y=0$ and the free boundary conditions corresponding to the lines $\{x=0,\ y=Y,\ x=X\}$ in the plane $\{z=0\}$. With these assumptions, equation (1) can be rewritten in the form

$$\frac{1}{c_0^2}\eta_{tt}=\Delta\eta+\frac{1}{c_0^2}f_{tt}(t,x,y).$$

This makes possible to consider the analytical solution of the above equation in the spectral domain. Let us denote

$$\overline{\eta}(x,y;\omega)=\int_{-\infty}^{\infty}\eta(x,y,t)e^{-i\omega t}\,dt,$$

$$\overline{f}(\omega,x,y)=\int_{-\infty}^{\infty}f(x,y,t)e^{-i\omega t}\,dt=\varphi(x,y)\int_{0}^{\infty}e^{-i\omega t}\,dt=\frac{-i}{\omega}\varphi(x,y).$$

After applying the Fourier transform with respect to time, one can obtain the following inverse problem: to recover the function $\varphi(x,y) \in L_2(\Omega)$ with a known spectrum of the function $\overline{\eta}(x,y;\omega)$ for a certain frequency band $[\omega_1, \omega_2]$

$$\overline{\eta}(x,y;\omega)|_M = \overline{\eta}_0(x_j, y_j, \omega), \quad \omega_1 \le \omega \le \omega_2 \tag{5}$$

with $\overline{\eta}(x,y;\omega)$ being the solution to the Helmholtz equation

$$\Delta\overline{\eta} + \frac{\omega^2}{h_0}\overline{\eta} = \frac{i\omega}{c_0}\varphi(x,y) \tag{6}$$

satisfying the Sommerfeld radiation condition. Therefore, the recorded field depends on the source amplitude in the following manner:

$$\overline{\eta}_0(x,y,\omega) = \frac{-i\omega}{c_0^2}\iint\limits_{\Omega} \varphi(\xi,\zeta) H_0^{(1)}\Big(k\sqrt{(x-\xi)^2+(y-\zeta)^2}\Big)\,d\xi\,d\zeta, \qquad i = 1,\dots,P, \tag{7}$$

where $k \equiv \omega/c_0$, and $H_0^{(1)}\Big(k\sqrt{(x-\xi)^2+(y-\zeta)^2}\Big)$ is Hankel's function. Let us denote $F(\omega) = -i\omega/c_0^2$. As was mentioned above, the trigonometric basis was chosen in the model space and the unknown function $\varphi(x,y)$ was sought for in the form (4). For the data space, let us consider that the observational system consists of P receivers disposed at a set of points $\{(x_i,y_i),\ i = 1,\dots,P\}$, where the spectrum of the recorded field $\overline{\eta}_0(x,y,\omega_j)$ is known for some frequency setting $\{\omega_j,\ j = 1,\dots,K_\omega\}$. This leads to the following system of linear algebraic equations with respect to the coefficients c_{mn} according to formula (4):

$$\overline{\eta}_0(x_i,y_i,\omega_j) = F(\omega_j)\sum_{m=1}^{M}\sum_{n=1}^{N} c_{mn}\int\limits_{x_1}^{x_M}\int\limits_{y_1}^{y_N} \sin\frac{m\pi}{l_1}(\xi - x_1)\sin\frac{n\pi}{l_2}(\zeta - y_1)\times H_0^{(1)}\Big(k_j\sqrt{(x_i-\xi)^2+(y_i-\zeta)^2}\Big)\,d\xi\,d\zeta. \tag{8}$$

In order to compute these integrals, the uniform grid was introduced over the rectangle Ω with the parameters R, Q over x and y directions, respectively: $h_x = l_1/R$, $h_y = l_2/Q$, $\xi_p = ph_x$, $p = 0,\dots,R$, $\zeta_q = qh_y$, $q = 0,\dots,Q$. Within each elementary rectangle $[\xi_p \le \xi \le \xi_p + h_x] \times [\zeta_q \le \zeta \le \zeta_q + h_y]$ the bilinear approximation for Hankel's function was used. Then system (8) could be rewritten in the form

$$\overline{\eta}_{0,ij} = F_j \sum_{m=1}^{M}\sum_{n=1}^{N} c_{mn} \sum_{p=1}^{R-1}\sum_{q=1}^{Q-1} \int_{\xi_p}^{\xi_p+h_x}\int_{\zeta_q}^{\zeta_q+h_y} \sin\frac{m\pi}{l_1}(\xi - x_1)\sin\frac{n\pi}{l_2}(\zeta - y_1) \times \tilde{H}_{pq}(\xi,\zeta)\,d\xi\,d\zeta. \tag{9}$$

Now, it is possible to use the $\boldsymbol{r}$-solution method for system (9) as was explained in [4].

There is another fact to be remarked: the vector $\overline{\eta}_0(x, y, \omega_j)$ is a complex one when the unknown function $\varphi(x, y)$ describing the source amplitudes is a real one. Therefore, the unknown coefficients $\{c_{mn}\}$ will be real, too. This fact was taken into account in the algorithm as follows: instead of every ith complex equation of system (9) there are written two real equations of the new system, where the $(2i-1)$th row will consist of a real component part of the ith rows of the "old" matrix and of the ith component part of the right-hand side vector of the "old" system. Similarly, the $(2i)$th row of the new matrix will correspond to the imaginary parts of the ith row of the matrix and the right-hand side vector, respectively. Thus, the number of equations in the new system (9) will be equal to $L = 2PK_w$.

3. Numerical experiments: description and discussion

A series of calculations were carried out by the method proposed to set up the dependence of the goodness of an inverted function on certain characteristics of the observational system such as the number and location of receivers, the frequency band of the data. As the main objective of our research is an application to reconstructing an initial tsunami waveform, we can assume the location of the target domain Ω to be known. In the truly real cases, the tsunami source area is specified from seismological data shortly after the event. Synthetic data for the numerical inversion experiments presented below were computed as a solution of problem (1), (2) with appropriate boundary conditions and a function $\varphi(x, y)$ in the form

$$\varphi(x, y) = \beta(x, y)\alpha(x), \tag{10}$$

where the parameter $\alpha(x)$ was selected according to the case study that will be clear in what follows. Let

$$\beta(x, y) = \max\left\{1 - \frac{(x-x_0)^2}{R_1^2} - \frac{(y-y_0)^2}{R_2^2}, 0\right\}. \tag{11}$$

The goodness of the reconstruction is estimated with a *misfit parameter* as a percentage relative error in the l_2-norm:

$$\left(\sum_{i=1}^{K}(\varphi_i-\hat{\varphi}_i)^2\right)^{1/2} \Big/ \left(\sum_{i=1}^{K}\varphi_i^2\right)^{1/2} \times 100\ \%, \quad K=NM;$$

the ratio of the squared averaged difference between the theoretical values $\{\varphi_i = \varphi(x_m, y_n),\ i = n + (m-1)N,\ n = 1, \ldots, N,\ m = 1, \ldots, M\}$ and the inverted ones to the theoretical function.

A series of the calculations were made by the method proposed and were aimed at recovering the unknown function $\varphi(x, y)$ in the form (4). Let us assume: a flat bathymetry $h(x, y) \approx 4.082$ (below all distances are scaled in kilometers); the wave velocity $c_0 = \text{const} = 0.2$ km/s; $\alpha(x) = 1$ in formula (10), i.e., the initial field is only a turning-up function. Let us denote a computational domain on the surface $\{z = 0\}$ as a rectangle $\Pi = \{(x, y) : -X \le x \le X,\ 0 \le y \le Y\}$ encompassing all the receivers and the source area Ω. We assume that the total reflective boundary condition (3) is fulfilled on the line $y = 0$, and an open boundary corresponds to the lines $x = -X$, $x = X$, $y = Y$. The center of the source is located at $(x_0, y_0) = (0, 150)$. The function $\varphi(x, y)$ is sought for according to formula (4) with $M = N = 21$, its maximum value being $\varphi_{\max} = 1$ m, and the domain Ω is a spatial discretization by means of 100×100 mesh points, i.e., $R = Q = 101$ in (9).

Let us define an assembly of the above specifying parameters as Pattern and designate as Model the parameters of Pattern joint with additional parameters such as the number of receivers K_p, the number of frequencies K_w, the range of frequency band and a geometry of aperture. Figure 1 shows the layout scheme of the source-receivers arrangement for Models 1–3 used below.

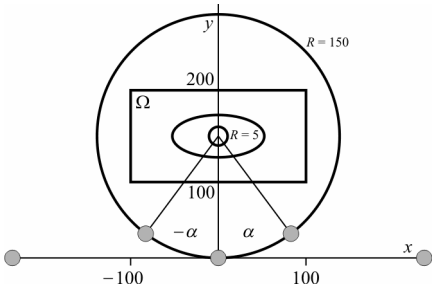

Figure 1. The source-receivers arrangement on the surface $z = 0$: the source for Model 1 is the central small circle, the source for Models 2 and 3 is the central ellipse, the target domain Ω is the rectangle; receivers are marked with bullets

The dependence of the inverted field on the number of receivers and the aperture angle. This issue is of primary practical importance: how goodness of the inverted function depends on the number of receivers used in the inversion procedure. First of all, our purpose was to obtain acceptable results of the inversion using a minimum number of *marigrams*. In this connection, we have made the computer simulation using a number of records that range from 1 to 30 with different azimuthal coverage.

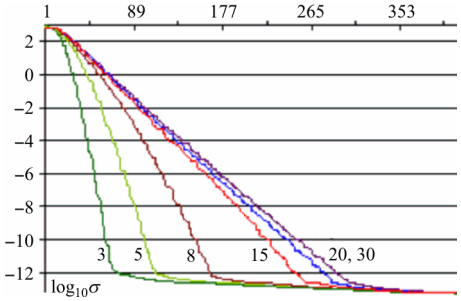

Figure 2. The singular spectra of the matrix A for Model 1 with different numbers of receivers used in the inversion

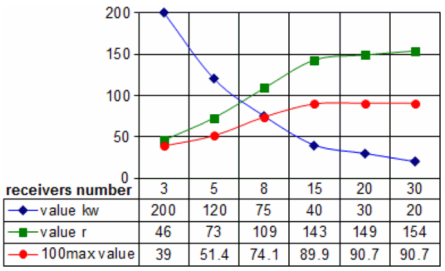

receivers number	3	5	8	15	20	30
value kw	200	120	75	40	30	20
value r	46	73	109	143	149	154
100max value	39	51.4	74.1	89.9	90.7	90.7

Figure 3. Dependence of the number $\boldsymbol{r}$, a maximum value of the inverted function and of the value K_w on the number of receivers in Model 1; cond $A = 10^8$

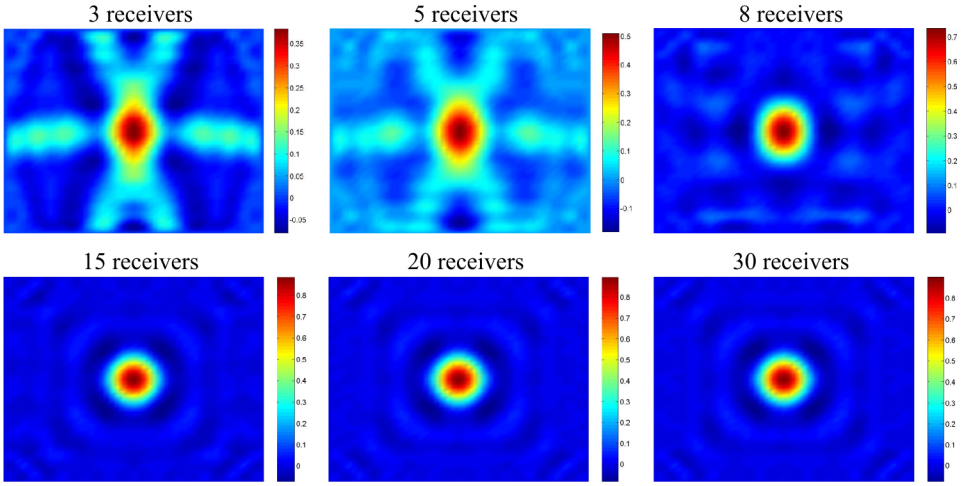

Figure 4. The inverted fields in Model 1

Let us consider *Model 1* based on Pattern with the linear aperture along the line $y = 0$, $L = 1000$ (according to Figure 1) and cond $A = 10^8$, the number of receivers being: 3, 5, 8, 15, 20, 30. These receivers were uniformly distributed along the aperture. Comparing the singular spectra for the different inversion versions in Figure 2 we can predict the best or a poor inversion: a worse result will be in the inversion in which 3 receivers were used, while the best result will be provided using 15–30 receivers (as will be clear in what follows, for a real bathymetry increasing the number of receivers will not ensure the better inversion). Indeed, Figure 3 shows the number $\boldsymbol{r}$, K_w and a maximum value of the inverted function multiplied by 100 against the number of the receivers used in the inversion. It should be mentioned that the value K_w in the experiments performed was defined by storing a product value $K_p K_w$. The goodness of a solution is improving when

the number of stations increases up to 15. Obviously, further increasing is useless. This is confirmed by the pictures of the inverted fields in Figure 4 (see maximum values of the inverted function in the table in Figure 3).

Within the scope of the model with a constant depth of the basin, the dependence of the goodness of the inversion on the number of receivers and their azimuthal envelopment was studied. Let us change some spatial parameters in Pattern. Let now the function $\varphi(x, y)$ be a semi-ellipsoid (10), (11) with $\alpha(x) = 1$, $R_1 = 50$, $R_2 = 25$; $w \in [0.001, 0.01]$ Hz; $\Omega = \{(x, y) : -100 \le x \le 100, 100 \le y \le 200\}$ and the number of receivers range is from 3 to 15 in *Model 2*, from 1 to 5 in *Model 3*, respectively.

Figure 1 above shows the arrangement of receivers: in Model 2 they are uniformly distributed on the line $y = 0$, $L = 200$, while in Model 3 receivers were set on the segment $[-\alpha, \alpha]$ of the circle centered at the point $(0, 150)$ with $R = 150$ and the aperture angle $\{2\alpha,\ \alpha = \pi n/10,\ n = 0.5, 1, 2.5, 3, 5, 6, 10\}$. It is clear from Figure 5 that the behavior of the singular spectra as a function of the number of receivers in Model 2 keeps the main features being typical of the ill-posed problem singular spectrum. Here, the quantity of frequencies K_w was equal 30 for the inversion by 15, 10, 7 marigrams; 50 for the case with 5 marigrams and 100 for the case with 3 marigrams, respectively. In Figure 6, the inverted fields within Model 2 are represented.

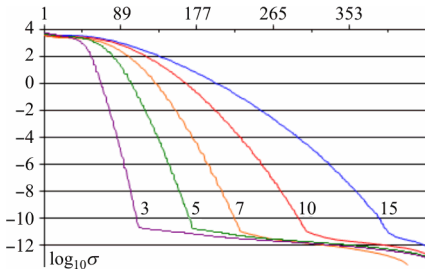

Figure 5. The singular spectra of the matrix A in Model 2 with different numbers of receivers used in the inversion

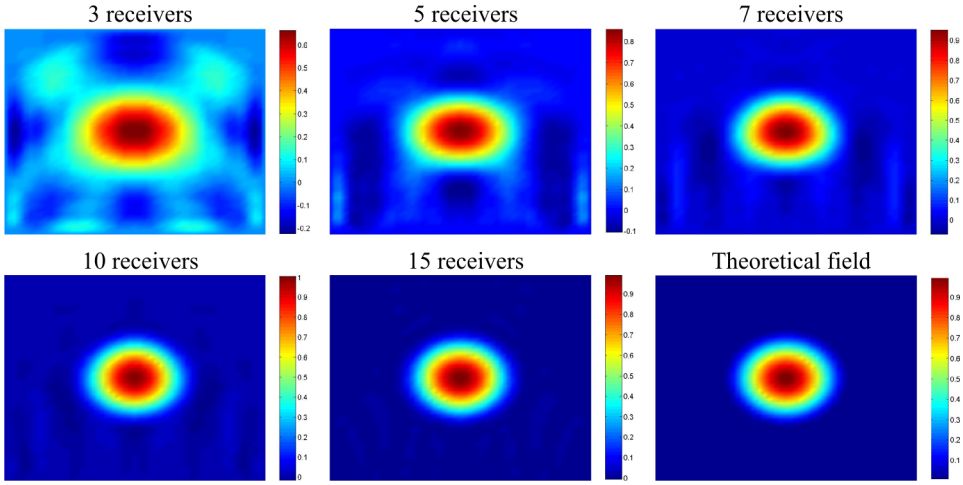

Figure 6. The inverted fields in Model 2

Next, we present the results obtained in Model 3 when the goodness of the inversion was studied with a range of the aperture angle and the number of receivers. In Figure 7, one can see how a singular spectrum of the matrix A changes with the number of receivers being increase from 1 to 5. In addition, the available interval of the number $\boldsymbol{r}$ is increasing and, as consequence, the inversion is improving. Adding new receivers leads to increasing a maximum value of the inverted function (line 4 in Figure 8) from the value 0.28 to the value 0.876 and, simultaneously, to decreasing the misfit parameter (line 2) from 44 % to 2.43 % for the cases with different aperture angles.

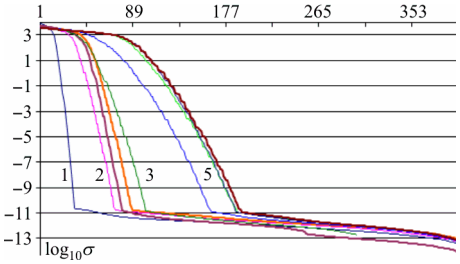

Figure 7. The singular spectra of the matrix A in Model 3 with the different aperture angle ranges

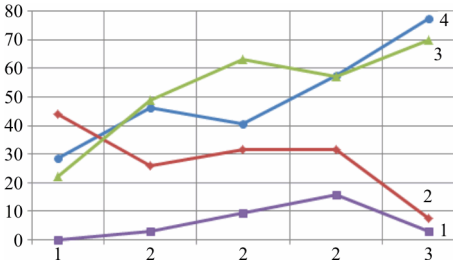

Figure 8. The diagram of changing the inversion parameters with the number of receivers used in the calculations in Model 3: an aperture angle multiplied by 10 (1), the misfit parameter (2), the number $\boldsymbol{r}$ (3) and the maximum value of the inverted function multiplied by 100 (4)

Figure 9 shows that other inversion parameters also obey the already obtained regularities: adding receivers to the inversions procedure leads to increasing the number $\boldsymbol{r}$ that results in obtaining a more informative solution, i.e., the inversions become more robust. The results represented in Figure 9 show that increasing the aperture angle leads to the rise of the maximum value of the inverted function (line 3). At the same time, the total volume of the displacement in the target domain (line 1) is invariant in all these cases in contrast to the total energy (line 2), as is shown in Figure 9.

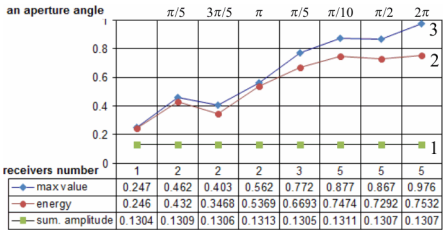

Figure 9

Let us discuss the results represented in Figure 10. When 5 receivers were used in the inversion process, the simulation was made not only with cond $A = 10^8$ (lines 3a and 2a), but, in addition, with cond $A = 100$ (lines 3b and 2b) for the misfit parameter and a maximum value of the inverted function, respectively. As it is clear from the graphs in Figure 10, the misfit parameter and maximum values of the inverted function are worse when

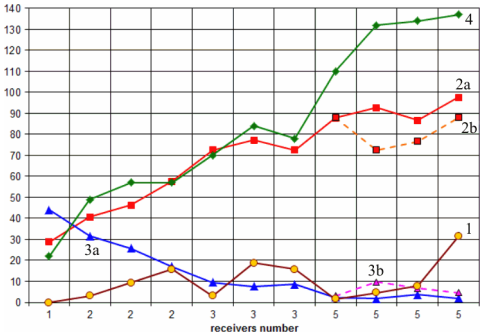

Figure 10. The diagram of changing the inversion parameters with the aperture angle range and the number of receivers used in Model 3: half-aperture angle multiplied by 10 (1); 100max (2a) and the misfit parameter (3a) for cond $A = 10^8$; the number $\boldsymbol{r}$ (4); and 100max (2b) and the misfit parameter (3b) for cond $A = 100$

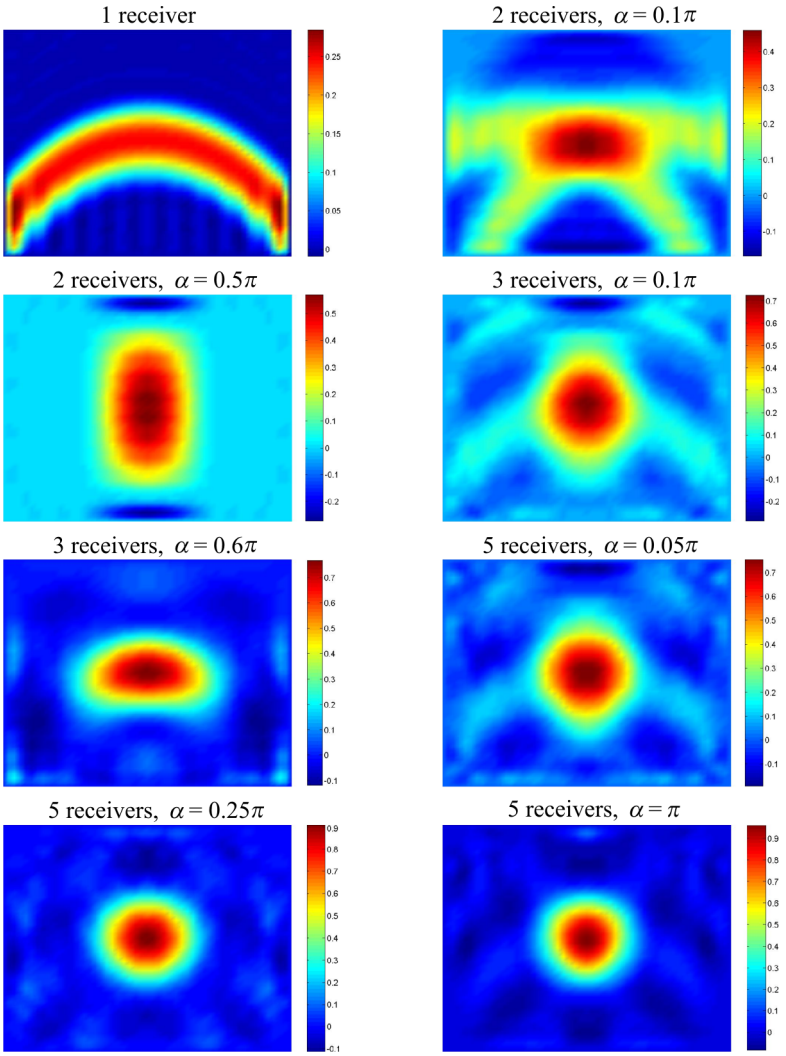

Figure 11. The inverted fields in Model 3

$\operatorname{cond} A = 100$. When the aperture angle (line 1) is sufficiently wide, the influence of the conditioning number is not significant.

The inverted fields for the cases that were discussed above are presented in Figure 11. The best result was obtained when the source area is ringed by receivers, i.e. the half-aperture angle $\alpha = \pi$ and the number of marigrams engaged in the inversion process is equal to 5.

4. Conclusion

We applied an inversion method to the problem of reconstructing the initial water elevation field that generates a tsunami. The application of $\boldsymbol{r}$-solutions is an effective means of regularization of an ill-posed problem. The number of $\boldsymbol{r}$ basic vectors applied appears to be essentially lower than the minimum dimension of the matrix. This, in fact, enables one to avoid the instability of the problem caused by a sharp decrease in singular values of the matrix. We have also shown that the quality of reconstruction depends, mainly, on the range of angles of observation. The best range is the entire circle. The quality of a solution is improving when the number of stations increase up to 10–15. The further increase is useless. Since the calculations were really made in the time-spectral domain, we can conclude that for the solution to be satisfactory, the shortest wavelength should be less than half the characteristic size of the tsunami source. The number of frequencies used in calculations should not be large; it is sufficient to use about 15 frequencies. This result should be kept in mind when designing a tide-gauge network to study a tsunami source.

References

[1] Satake K. Inversion of tsunami waveforms for the estimation of a fault heterogeneity: method and numerical experiments // J. Phys. Earth. — 1987. — Vol. 35. — P. 241–254.

[2] Pires C., Miranda P.M.A. Tsunami waveform inversion by adjoint methods // J. Geophys. Res. — 2001. — Vol. 106, No. C6. — P. 19773–19796.

[3] Tinti S., Piatanesi A., Bortolucci E. The finite-element wavepropagator approach and the tsunami inversion problem // J. Phys. Chem. Earth. — 1996. — Vol. 12. — P. 27–32.

[4] Voronina T.A., Tcheverda V.A. Reconstruction of tsunami initial form via level oscillation // Bull. Novosibirsk Comp. Center. Ser. Math. Model. in Geoph. — Novosibirsk, 1998. — Iss. 4. — P. 127–136.

[5] Voronina T.A. Determination of spatial distribution of oscillation sources by remote measurements on a finite set of points // Sib. J. Num. Math. — 2004. — Vol. 3. — P. 203–211.

[6] Cheverda V.A., Kostin V.I. r-pseudoinverse for compact operator // Siberian Electronic Mathematical Reports. — 2010. — Vol. 7. — P. 258–282.

[7] Voronina T.A. Reconstruction of initial tsunami waveforms by a trancated SVD method // J. Inverse and Ill-posed Problems. — 2011. — Vol. 19. — P. 615–629.

[8] Voronina T.A. Application of r-solutions to reconstructing an initial tsunami waveform // Numerical Methods and Programming. Scientific On-Line Open Access Journal. — 2013. — Vol. 14. — P. 165–174.